Low-frequency charge noise in Si/SiGe quantum dots

Elliot J. Connors,[1] JJ Nelson,[1] Haifeng Qiao,[1] Lisa F. Edge,[2] and John M. Nichol[1,*]
[1]*Department of Physics and Astronomy, University of Rochester, Rochester, New York 14627, USA*
[2]*HRL Laboratories LLC, 3011 Malibu Canyon Road, Malibu, California 90265, USA*

(Received 25 July 2019; revised manuscript received 26 September 2019; published 23 October 2019)

Electron spins in silicon have long coherence times and are a promising qubit platform. However, electric field noise in semiconductors poses a challenge for most single- and multiqubit operations in quantum-dot spin qubits. We investigate the dependence of low-frequency charge noise spectra on temperature and aluminum-oxide gate dielectric thickness in Si/SiGe quantum dots with overlapping gates. We find that charge noise increases with aluminum-oxide thickness. We also find strong dot-to-dot variations in the temperature dependence of the noise magnitude and spectrum. These findings suggest that each quantum dot experiences noise caused by a distinct ensemble of two-level systems, each of which has a nonuniform distribution of thermal activation energies. Taken together, our results suggest that charge noise in Si/SiGe quantum dots originates at least in part from a nonuniform distribution of two-level systems near the surface of the semiconductor.

DOI: 10.1103/PhysRevB.100.165305

I. INTRODUCTION

Electron spins in silicon quantum dots are a promising platform for quantum computation [1–8]. Long coherence times enable high-fidelity qubit operations required for universal quantum computing. Although silicon qubits largely avoid nuclear spin noise, charge noise in the semiconductor still limits both single- and multiqubit gate fidelities. Moreover, charge-noise levels appear to be similar in different silicon devices and materials [4,9–15]. Because noise mitigation strategies such as device engineering, dynamical decoupling [16,17], and dynamically corrected gates [18] rely on a detailed understanding of the noise, a thorough characterization of charge noise is essential.

Here, we characterize the low-frequency charge noise in Si/SiGe quantum dots with overlapping gates [19,20]. We investigate the dependence of the charge-noise spectrum on temperature and Al_2O_3 gate-oxide thickness. We generally find that the noise increases with the aluminum oxide thickness. Although on average the noise follows a $1/f$ power law with a linear temperature dependence, we find strong dot-to-dot variations in the noise spectrum. As we discuss below, we suggest that each quantum dot experiences noise caused by an ensemble of two-level systems (TLSs). Furthermore, we suggest that separate quantum dots experience noise caused by different TLS ensembles, each of which has a different and nonuniform distribution of thermal activation energies. In turn, variations in the TLS ensembles between dots give rise to the dot-to-dot variations in the noise. Specifically, we analyze our measurements in the context of the Dutta-Horn (DH) model [21], which considers noise generated by a nonuniform distribution of TLSs, and we find good qualitative agreement with our data. In light of these findings, we conclude that charge noise in Si/SiGe quantum dots is caused, at least in part, by a nonuniform distribution of two-level systems near the surface of the semiconductor.

II. CHARGE NOISE MEASUREMENTS

Devices are fabricated on an undoped Si/SiGe heterostructure with an 8-nm-thick Si quantum well approximately 50 nm below the surface and a 4 nm Si cap, which forms a thin native SiO_2 layer on its surface. Voltages applied to three layers of electrostatically isolated overlapping aluminum gates defined with electron beam lithography accumulate and confine electrons in the Si quantum well forming the quantum dots [Figs. 1(a) and 1(b)] [19,20].

Prior to quantum-dot fabrication, we deposit Al_2O_3 on the entire wafer surface via atomic layer deposition. On certain devices, we remove some or all of the Al_2O_3 in the device region, allowing us to adjust the thickness of the gate dielectric. Table I shows the parameters of the devices used here. On device 1, we nominally removed all of the Al_2O_3 with H_3PO_4 (Transene Transetch-N), which selectively etches Al_2O_3 compared with SiO_2. We did not attempt to modify the native SiO_2 layer. We also note that deposition of aluminum gates directly on an Al_2O_3 or SiO_2 surface leads to interfacial layers of AlO_x and modification of the underlying oxide [22,23]. It is therefore likely that a few nm of additional AlO_x exists underneath the aluminum gates on all devices, including device 1, where we remove the deposited Al_2O_3 by wet etch. In the following, we will refer to the deposited Al_2O_3 layer that exists over the device region as the gate oxide [Fig. 1(b)]. We measured the gate-oxide thicknesses with a combination of white-light optical reflectometry, contact profilometry, and atomic force microscopy. See Supplemental Material [24] for further device fabrication details.

All devices are cooled in a dilution refrigerator with a base temperature of approximately 50 mK and then tuned to the Coulomb blockade regime [Fig. 1(c)]. We apply a

*jnich10@ur.rochester.edu

 ©2019 American Physical Society

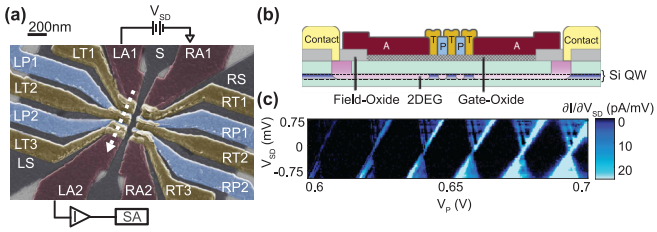

FIG. 1. Experimental setup. (a) False color scanning electron microscope image of an overlapping-gate quantum-dot device identical to those measured. Dots are formed under plunger gates (blue) using screening gates (dark gray) and tunneling gates (yellow) to confine the electrons in the underlying two-dimensional electron gas (2DEG). A source drain bias V_{SD} is applied to the 2DEG to drive a current (dashed white arrow) through the dot. Current is measured with a current preamplifier and a spectrum analyzer (SA). (b) Cross section of the device along the current path. The gate oxide consists of Al_2O_3 grown by atomic layer deposition. (c) Differential conductance $\partial I/\partial V_{SD}$ showing representative Coulomb blockade diamonds.

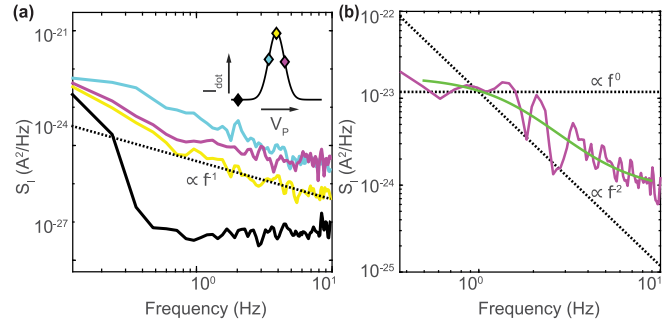

FIG. 2. Noise spectrum measurement. (a) Current noise power spectral density measurement. Charge noise is measured by acquiring current noise spectra with the plunger gate V_P set on both sides of a transport peak where $|dI/dV_P|$ is large, as shown in the inset. Additional spectra are measured with V_P set within the Coulomb blockade region for a baseline measurement of our experimental setup, and with V_P set on top of the peak where $|dI/dV_P|$ is small as a check to ensure that the measurement is sensitive to charge noise. A dashed trendline proportional to f^{-1} is shown. (b) Measured current noise spectrum showing non-power-law behavior (magenta). The green line is a fit of the measured data to a function of the form $\frac{A}{f^\beta} + \frac{B}{f^2/f_0^2+1}$, where A, B, β, and f_0 are fit parameters. Dashed lines proportional to f^0 and f^{-2} are shown.

filtered source-drain bias of less than 1 mV across the device and measure the current I with an SR570 low-noise current preamplifier. Current noise spectra are acquired on an SR760 spectrum analyzer with the plunger gate voltage V_P set on the left, right, and top of a transport peak, as well as in the Coulomb blockade regime where $I = 0$ [Fig. 2(a)]. We observe that the current fluctuations are most pronounced on the sides of the peak, where $|dI/dV_P|$ is largest, indicating that electrochemical potential fluctuations make the dominant contribution to current noise [9,25].

In the regime where chemical potential fluctuations dominate the current noise, small current fluctuations δI are given by

$$\delta I = \frac{dI}{dV_P}\frac{\delta_\epsilon}{\alpha}, \tag{1}$$

where $\delta\epsilon$ is a small change in the electrochemical potential and α is the lever arm. We extract dI/dV_P from a fit of the transport peak and use Eq. (1) to convert the acquired current noise spectrum S_I to a charge noise spectrum S_ϵ via the relationship

$$S_\epsilon = \frac{\alpha^2 S_I}{|dI/dV_P|^2}. \tag{2}$$

Note that Eq. (1) applies only when $\delta\epsilon \ll \Delta\epsilon$, where $\Delta\epsilon$ is the width of the transport peak [26]. When $\delta\epsilon \approx \Delta\epsilon$, Eq. (2) underestimates the charge noise. Based on simulations, we estimate that measured values of S_ϵ differ from actual values by at most a factor of approximately 1.4 at low temperature (see Supplemental Material [24] for simulation details). Lever arms are extracted from Coulomb diamond measurements [Fig. 1(c)] and, when possible, confirmed from a fit of the transport peak width versus temperature. Lever arms range from 0.036 to 0.092 eV/V, with smaller lever arms corresponding to quantum dots in devices with more gate oxide (see Supplemental Material [24] for lever arm extraction details).

Generally, the measured charge-noise spectra have a power-law frequency dependence [Fig. 2(a)]. However, some spectra are better described by the sum of a power law and a Lorentzian [Fig. 2(b)]. Spectra of this type are observed on all devices. As we discuss below, Lorentzian noise spectra suggest the presence of individual or small numbers of TLSs.

We fit the measured $S_\epsilon(f)$ to a function of the form $\frac{A}{f^\beta} + \frac{B}{f^2/f_0^2+1}$, which is the sum of a power law and a Lorentzian,

TABLE I. Parameters of devices measured at the base temperature of our dilution refrigerator. Quantum dots are specified by the plunger gate beneath which they exist, as shown in Fig. 1(a). For example, QD R1 is formed underneath plunger gate RP1. Values of α labeled with an asterisk have been verified via a fit of the transport peak width vs temperature. Values for $S_\epsilon^{1/2}(1\text{ Hz})$ are given for both individual dots and for each device. The reported value of the average $S_\epsilon^{1/2}(1\text{ Hz})$ at each dot is calculated by averaging all measurements taken on that respective dot at the base temperature of the dilution refrigerator.

Device	Gate oxide (nm)	QD	α (eV/V)	$S_\epsilon^{1/2}(1\text{ Hz})$ ($\mu\text{eV}/\sqrt{\text{Hz}}$) QD Avg.	Device Avg.
1	0	R1	0.088*	0.89	0.84 ± 0.04
		L1	0.092*	0.77	
		L2	0.070*	0.87	
2	15	R1	0.073*	1.04	0.93 ± 0.18
		L1	0.080*	0.59	
		L2	0.073*	1.17	
3	46	R1	0.048	1.87	1.77 ± 0.09
		R2	0.036	1.84	
		L1	0.038	1.59	

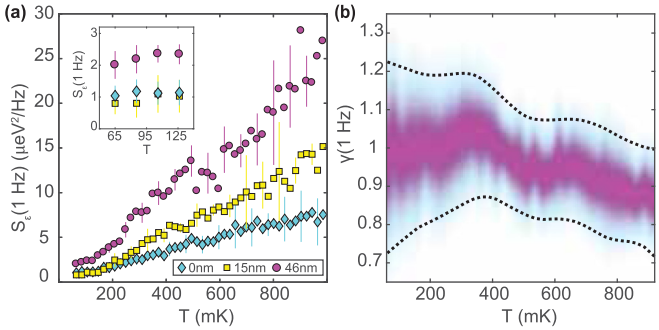

FIG. 3. Temperature dependence of the charge noise. (a) Plot of the averaged $S_\epsilon(1\ \mathrm{Hz})$ vs temperature across three different samples with 0, 15, and 46 nm of gate oxide. Measurements of $S_\epsilon(1\ \mathrm{Hz}, T)$ were made on three quantum dots on device 1, two quantum dots on device 2, and one quantum dot on device 3. The inset shows the same data near the base temperature of the dilution refrigerator. The data show a clear trend of increasing noise with gate-oxide thickness, especially at high temperature. Error bars are included on every third point and represent the standard error in the mean. (b) Plot of the spread of $\gamma(1\ \mathrm{Hz}, T)$ of all measured samples. The colored shadow represents the distribution of $\gamma(1\ \mathrm{Hz})$ at a given temperature, and is centered about the mean value. The dashed lines indicate one standard deviation above and below the mean.

from 0.5 to 9 Hz. Here A, B, β, and f_0 are fit parameters. From this fit we directly extract the charge noise at 1 Hz, $S_\epsilon^{1/2}(1\ \mathrm{Hz})$, and we also obtain the frequency exponent at 1 Hz, $\gamma = -\partial \ln S_\epsilon / \partial \ln f|_{f=1\,\mathrm{Hz}}$, by differentiating the fit at 1 Hz. In total, we measured noise spectra on quantum dots on three separate devices with gate-oxide thicknesses of 0, 15, and 46 nm. At the base temperature of our dilution refrigerator, we measured three quantum dots on each device to find $S_\epsilon^{1/2}(1\ \mathrm{Hz})$ to be $0.84 \pm 0.04\ \mu\mathrm{eV}/\sqrt{\mathrm{Hz}}$ on device 1 (0 nm gate oxide), $0.94 \pm 0.18\ \mu\mathrm{eV}/\sqrt{\mathrm{Hz}}$ on device 2 (15 nm gate oxide), and $1.77 \pm 0.09\ \mu\mathrm{eV}/\sqrt{\mathrm{Hz}}$ on device 3 (46 nm gate oxide). A compilation of device parameters and charge noise values is given in Table I. At base temperature, the charge noise generally increases with the gate-oxide thickness. We discuss this observation further below.

We investigate the temperature dependence of the charge noise at 1 Hz by sweeping the sample temperature from 50 mK to 1 K in fine-grained step sizes ranging from 2 to 10 mK, with larger step sizes used at higher temperatures. Temperature sweeps were conducted on three quantum dots on device 1, two quantum dots on device 2, and one quantum dot on device 3. Figure 3(a) shows the average temperature dependence of $S_\epsilon(1\ \mathrm{Hz})$ for devices with varying gate-oxide thicknesses, averaged across all quantum dots measured on each device. Again, we see that the noise increases with the gate-oxide thickness, especially at high temperature. Figure 3(b) shows the spread in $\gamma(1\ \mathrm{Hz})$ as a function of temperature. See Supplemental Material at [24] for a detailed description of the analysis of the measured data.

Although on average the charge noise is approximately $1/f$ and varies approximately linearly with temperature, there is significant dot-to-dot variation in the temperature dependence of S_ϵ and γ. This is especially pronounced at low temperatures. In some cases, the temperature dependence of the noise experienced by a quantum dot differs depending on which side of a transport peak V_P is set [Figs. 4(b) and 4(c)].

III. ANALYSIS OF LOW-FREQUENCY CHARGE NOISE

It is generally thought that $1/f$ noise in semiconductors results from a distribution of bistable charge states. Such fluctuators are regularly observed in various solid-state platforms [25,27–37]. A simple model for TLSs causing $1/f$ noise proposed by McWhorter [38] considers a distribution of TLSs, each of which switches between two states and contributes a Lorentzian power spectrum to the overall noise spectrum. Under the assumption that τ, the switching time of the TLSs, is thermally activated such that $\tau = \tau_0 e^{E/k_BT}$, the spectrum of a single TLS is given by

$$s_\epsilon(f, T) = \frac{\tau_0 e^{E/k_BT}}{4\pi^2 f^2 \tau_0^2 e^{2E/k_BT} + 1}. \tag{3}$$

Here, E and τ_0 are the activation energy and the characteristic attempt time of the TLS, respectively. The total power spectrum, $S_\epsilon(f, T)$, is simply the integral of all TLS power spectra over a distribution of activation energies $D(E)$,

$$S_\epsilon(f, T) = \int \frac{\tau_0 e^{E/k_BT}}{4\pi f^2 \tau_0^2 e^{2E/k_BT} + 1} D(E) dE. \tag{4}$$

If the distribution of TLS activation energies, $D(E)$, is constant, one arrives at a total noise spectrum that is proportional to k_BT/f [38].

As shown in Fig. 4, however, data from individual dots show strong deviations from a $1/f$ spectrum and linear temperature dependence. Nonlinear temperature dependence and anomalous frequency dependence of the charge noise have also previously been observed in semiconductor quantum dots [10,39,40]. In the following, we describe how a nonuniform distribution of TLSs can give rise to this behavior. One might generally expect a nonuniform distribution of TLSs to result in anomalous temperature and spectral dependence of the noise. Consider, for example, a single TLS with a Lorentzian noise spectrum. On the one hand, for frequencies $f \ll 1/2\pi\tau$ the noise is white and decreases exponentially with temperature ($\tau = \tau_0 e^{E/k_BT}$ is the temperature-dependent switching time). On the other hand, for frequencies $f \gg 1/2\pi\tau$ the noise varies as f^{-2} and increases exponentially with temperature.

The model of Dutta and Horn [21] extends the McWhorter model to account for a nonuniform distribution of TLSs. The DH model has successfully described $1/f$ noise in a large variety of solid-state systems [21,41–43]. Under the assumption that the width of the distribution of activation energies is larger than k_BT, one can expand the result of Eq. (4) in powers of T to obtain

$$S_\epsilon(f, T) = \frac{k_BT}{2\pi f} D(\tilde{E}), \tag{5}$$

where $\tilde{E} = -k_BT \ln(2\pi f \tau_0)$. Equation (5) shows that if $D(E)$ is not constant, then $S_\epsilon(f, T)$ will not vary linearly with temperature. Additionally, if $\gamma \neq 1$, then Eq. (5) suggests $D(\tilde{E})$ must not be constant. Moreover, by defining $\gamma \equiv -\partial \ln S_\epsilon / \partial \ln f$, one can use Eq. (5) to obtain the following

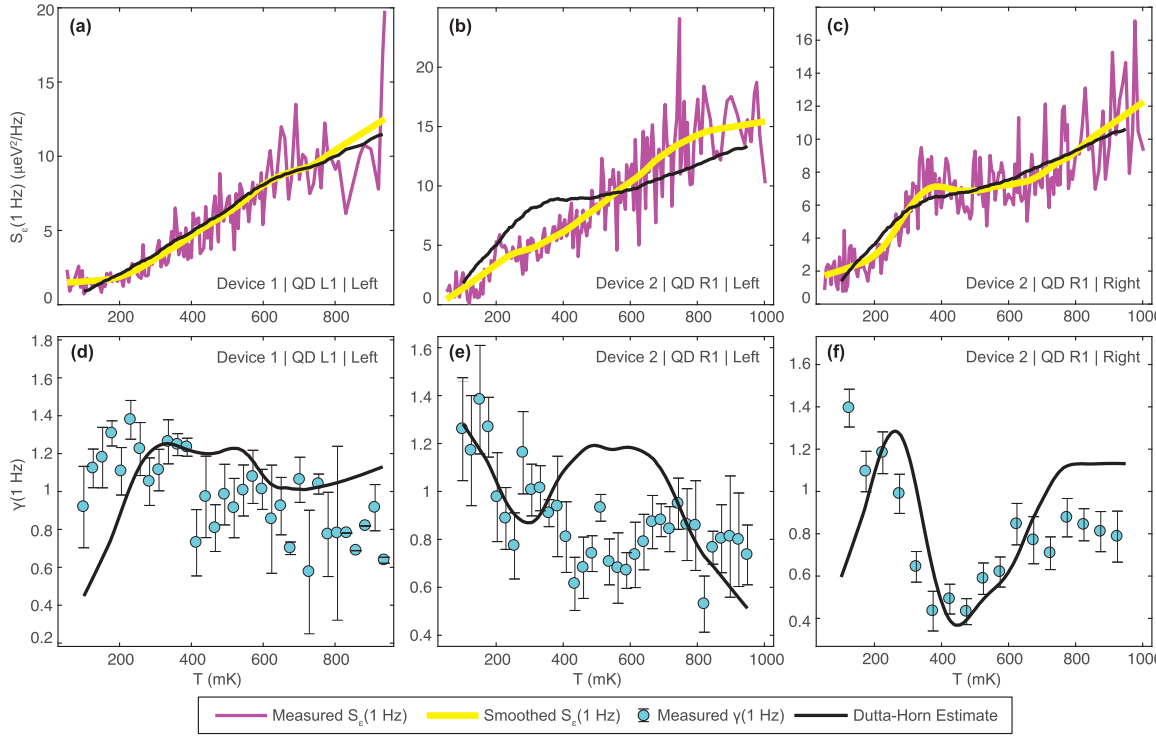

FIG. 4. Measured temperature dependence of the noise magnitude and exponent. (a) $S_\epsilon(1\,\mathrm{Hz})$ vs temperature on the left side of a transport peak for quantum dot L1 on device 1. (b) $S_\epsilon(1\,\mathrm{Hz})$ vs temperature on the left side of a transport peak for dot R1 on device 2. (c) $S_\epsilon(1\,\mathrm{Hz})$ vs temperature on the right side of a transport peak for dot R1 on device 2. (d) Averaged measurements of $\gamma(1\,\mathrm{Hz})$ vs temperature on the left side of the transport peak for dot L1 on device 1. (e) Averaged measurements of $\gamma(1\,\mathrm{Hz})$ vs temperature on the left side of the transport peak for dot R1 on device 2. (f) Averaged measurements of $\gamma(1\,\mathrm{Hz})$ vs temperature on the right side of the transport peak for dot R1 on device 2. The smooth yellow lines are generated by taking a moving average of the data. The black lines in (a), (b), and (c) are the estimates for $S_\epsilon(1\,\mathrm{Hz}, T)$ using Eq. (6) of the Dutta-Horn model and the data in (d), (e), and (f), respectively. Error bars in (d), (e), and (f) represent the standard error associated with averaging the data over temperature ranges of 25 mK. The solid lines in (d), (e), and (f) are estimates for $\gamma(1\,\mathrm{Hz}, T)$ using Eq. (6) of the Dutta-Horn model and the smoothed yellow lines in (a), (b), and (c), respectively.

relation between the noise power $S_\epsilon(f, T)$ and the frequency exponent $\gamma(f, T)$:

$$\gamma(f, T) = 1 - \frac{1}{\ln(2\pi f \tau_0)}\left[\frac{\partial \ln S_\epsilon(f, T)}{\partial \ln T} - 1\right]. \quad (6)$$

Equations (5) and (6) are the basis of the DH model. Equation (5) relates the temperature dependence of the noise to the density of the TLSs. Equation (6) relates the temperature dependence of the frequency exponent to that of the noise magnitude. Note that Eq. (6) implies that deviations from $\gamma = 1$ imply a nonuniform distribution of TLSs and a nonlinear temperature dependence of $S_\epsilon(f, T)$ as discussed above. Figure 4 shows representative plots of our measurements of $S_\epsilon(1\,\mathrm{Hz}, T)$ and $\gamma(1\,\mathrm{Hz}, T)$. All data sets show deviations from both $\gamma = 1$ and the linear temperature dependence of $S_\epsilon(1\,\mathrm{Hz}, T)$.

According to the DH model, these data suggest a nonuniform distribution of activation energies $D(E)$. We show that our data are in qualitative agreement with the DH model in several ways. First, using the measurements of $\gamma(1\,\mathrm{Hz}, T)$, we integrate Eq. (6) to generate a prediction for $S_\epsilon(1\,\mathrm{Hz}, T)$. We generally observe good qualitative agreement with our measurements of $S_\epsilon(1\,\mathrm{Hz}, T)$ using this approach, although some of the sharp features are not perfectly captured [Figs. 4(a)–4(c)]. Second, to generate a predicted form of $\gamma(1\,\mathrm{Hz}, T)$ from our measured noise power spectral density, we smooth the data using a moving 50-point average. We then take the logarithmic derivative of the smoothed line to extract a prediction for $\gamma(1\,\mathrm{Hz}, T)$ based on Eq. (6) [see Supplemental Material at [24] for details regarding generating predictions for $S_\epsilon(1\,\mathrm{Hz}, T)$ and $\gamma(1\,\mathrm{Hz}, T)$ via the DH model]. Again, our predictions based on the DH model show reasonable qualitative agreement with the data [Figs. 4(d)–4(f)]. In all cases, we fixed the maximum attempt frequency $\omega_0 = 1/\tau_0$ at 5 s^{-1} to maximize the fit quality across all data sets. The required value of ω_0, which controls the size of the deviations from $\gamma = 1$ and the linear temperature dependence in the DH model, is puzzling because $1/f$ noise has been observed at higher frequencies in Si/SiGe quantum dots [4,14]. One possible explanation is that the assumptions of the DH model are not entirely satisfied in our experiment. For example, the presence of sharp features in the activation energy distribution, as suggested by individual Lorentzian features in the measured spectra, may cause strong deviations from $\gamma = 1$. However, we note that predictions of the DH model depend logarithmically on ω_0, so our results depend only weakly on its precise value.

Figure 4 shows the predictions for $S_\epsilon(1\,\mathrm{Hz}, T)$ and $\gamma(1\,\mathrm{Hz}, T)$ made by the DH model for three representative cases with varying quality of agreement between

measurements and predictions. Given the generally good qualitative agreement between our data and the DH predictions, we suggest that the charge noise results from a nonuniform distribution of TLSs. We note that the observation of Lorentzian features in the noise spectra corroborate this view [Fig. 2(b)]. See Supplemental Material at [24] for comparisons between our data and the DH model for all devices measured.

IV. NOISE CORRELATION MEASUREMENT

We obtain further insight into the nature of the noise source by measuring the temporal correlation of the charge noise on two neighboring quantum dots. First, we tune dots L1 and R1 on device 2 to the Coulomb blockade regime. We set both plunger gates to the sides of their respective transport peaks, and we acquire a time series of current fluctuations on each dot simultaneously for 3200 seconds and we repeat this procedure 20 times. We calculate correlation coefficients of the current fluctuations between dots for each 3200-second time series and average the result across the 20 repetitions, and we find a correlation coefficient $\rho(\delta I_{\mathrm{L1}}, \delta I_{\mathrm{R1}}) = -0.006 \pm 0.032$, which indicates that the noise at each dot is independent and local. See Supplemental Material at [24] for details regarding the calculation of the correlation coefficient. Together with our earlier results, it seems plausible that charge noise is caused by a small number of TLSs in close proximity to each quantum dot.

V. CONCLUSIONS

Our data suggest several possible explanations for the charge noise. One explanation is that the aluminum oxide itself contains the TLSs. In this case, we would expect that reducing the oxide thickness would reduce the overall noise. It is also possible that the TLSs exist in the semiconductor near its surface or at the SiO_2/AlO_x interface, and decreasing the aluminum oxide thickness improves screening effects from the metallic gates. If the individual TLSs consist of dipole charge traps [44–47], however, the metal gates will only screen dipoles oriented parallel to the surface. Image charges associated with dipoles oriented perpendicular to the surface would increase their contribution to the noise. For randomly oriented dipoles, one would not expect a significant change in the noise as the distance to the metal gates decreases. Thus, we suggest that the charge noise is caused at least in part by TLSs in the aluminum oxide, or dipole TLSs oriented parallel to the wafer surface and located either in the semiconductor near its surface or at the SiO_2/AlO_x interface. However, it seems more likely that interface TLSs would be oriented parallel to the wafer surface than TLSs in the bulk of the semiconductor. In all of these cases, we emphasize that reducing the AlO_x thickness is expected to reduce the noise, as suggested by this and previous work [48].

In summary, we find that the presence of an aluminum-oxide gate dielectric layer tends to increase charge noise in Si/SiGe quantum dots. We observe that most quantum dots on a given device suffer from similar levels of noise, though there often exist significant dot-to-dot variations in the temperature dependence of the noise across dots in the same device. In the context of the Dutta-Horn model, our findings suggest that a nonuniform distribution of TLSs is responsible for the charge noise. Based on our results, it seems plausible that a small number of TLSs near the surface of the semiconductor or in the gate oxide cause the charge noise. Our data underscore the importance of controlling defect densities in the gate stack on top of silicon quantum dots. Our results also emphasize the importance of fully characterizing the charge noise of individual quantum dots to determine optimal spin qubit dynamical decoupling protocols. Furthermore, we suggest the use of as little aluminum oxide as possible in the active region of Si/SiGe spin qubits as an effective means to reduce charge noise.

ACKNOWLEDGMENTS

Research was sponsored by the Army Research Office and was accomplished under Grants No. W911NF-16-1-0260 and No. W911NF-19-1-0167. The views and conclusions contained in this document are those of the authors and should not be interpreted as representing the official policies, either expressed or implied, of the Army Research Office or the U.S. Government. The U.S. Government is authorized to reproduce and distribute reprints for Government purposes notwithstanding any copyright notation herein. E.J.C. was supported by ARO and LPS through the QuaCGR Fellowship Program.

[1] M. Veldhorst, J. Hwang, C. Yang, A. Leenstra, B. de Ronde, J. Dehollain, J. Muhonen, F. Hudson, K. M. Itoh, A. Morello *et al.*, Nat. Nanotechnol. **9**, 981 (2014).

[2] A. M. Tyryshkin, S. Tojo, J. J. Morton, H. Riemann, N. V. Abrosimov, P. Becker, H.-J. Pohl, T. Schenkel, M. L. Thewalt, K. M. Itoh *et al.*, Nat. Mater. **11**, 143 (2012).

[3] A. Morello, J. J. Pla, F. A. Zwanenburg, K. W. Chan, K. Y. Tan, H. Huebl, M. Möttönen, C. D. Nugroho, C. Yang, J. A. van Donkelaar *et al.*, Nature (London) **467**, 687 (2010).

[4] J. Yoneda, K. Takeda, T. Otsuka, T. Nakajima, M. R. Delbecq, G. Allison, T. Honda, T. Kodera, S. Oda, Y. Hoshi *et al.*, Nat. Nanotechnol. **13**, 102 (2018).

[5] K. Eng, T. D. Ladd, A. Smith, M. G. Borselli, A. A. Kiselev, B. H. Fong, K. S. Holabird, T. M. Hazard, B. Huang, P. W. Deelman *et al.*, Sci. Adv. **1**, e1500214 (2015).

[6] B. M. Maune, M. G. Borselli, B. Huang, T. D. Ladd, P. W. Deelman, K. S. Holabird, A. A. Kiselev, I. Alvarado-Rodriguez, R. S. Ross, A. E. Schmitz *et al.*, Nature (London) **481**, 344 (2012).

[7] T. Watson, S. Philips, E. Kawakami, D. Ward, P. Scarlino, M. Veldhorst, D. Savage, M. Lagally, M. Friesen, S. Coppersmith *et al.*, Nature (London) **555**, 633 (2018).

[8] M. Veldhorst, C. Yang, J. Hwang, W. Huang, J. Dehollain, J. Muhonen, S. Simmons, A. Laucht, F. Hudson, K. M. Itoh *et al.*, Nature (London) **526**, 410 (2015).

[9] B. M. Freeman, J. S. Schoenfield, and H. Jiang, Appl. Phys. Lett. **108**, 253108 (2016).

[10] L. Petit, J. M. Boter, H. G. J. Eenink, G. Droulers, M. L. V. Tagliaferri, R. Li, D. P. Franke, K. J. Singh, J. S. Clarke, R. N. Schouten, V. V. Dobrovitski, L. M. K. Vandersypen, and M. Veldhorst, Phys. Rev. Lett. **121**, 076801 (2018).

[11] P. Harvey-Collard, N. T. Jacobson, M. Rudolph, J. Dominguez, G. A. Ten Eyck, J. R. Wendt, T. Pluym, J. K. Gamble, M. P. Lilly, M. Pioro-Ladrière *et al.*, Nat. Commun. **8**, 1029 (2017).

[12] Z. Shi, C. B. Simmons, D. R. Ward, J. R. Prance, R. T. Mohr, T. S. Koh, J. K. Gamble, X. Wu, D. E. Savage, M. G. Lagally, M. Friesen, S. N. Coppersmith, and M. A. Eriksson, Phys. Rev. B **88**, 075416 (2013).

[13] X. Wu, D. R. Ward, J. Prance, D. Kim, J. K. Gamble, R. Mohr, Z. Shi, D. Savage, M. Lagally, M. Friesen *et al.*, Proc. Natl. Acad. Sci. (USA) **111**, 11938 (2014).

[14] X. Mi, S. Kohler, and J. R. Petta, Phys. Rev. B **98**, 161404(R) (2018).

[15] M. Fogarty, K. Chan, B. Hensen, W. Huang, T. Tanttu, C. Yang, A. Laucht, M. Veldhorst, F. Hudson, K. M. Itoh *et al.*, Nat. Commun. **9**, 4370 (2018).

[16] L. Viola, E. Knill, and S. Lloyd, Phys. Rev. Lett. **82**, 2417 (1999).

[17] M. J. Biercuk, H. Uys, A. P. VanDevender, N. Shiga, W. M. Itano, and J. J. Bollinger, Nature (London) **458**, 996 (2009).

[18] X. Wang, L. S. Bishop, J. Kestner, E. Barnes, K. Sun, and S. D. Sarma, Nat. Commun. **3**, 997 (2012).

[19] D. Zajac, T. Hazard, X. Mi, K. Wang, and J. Petta, Appl. Phys. Lett. **106**, 223507 (2015).

[20] S. J. Angus, A. J. Ferguson, A. S. Dzurak, and R. G. Clark, Nano Lett. **7**, 2051 (2007).

[21] P. Dutta, P. Dimon, and P. M. Horn, Phys. Rev. Lett. **43**, 646 (1979).

[22] W. Lim, H. Huebl, L. Willems van Beveren, S. Rubanov, P. Spizzirri, S. Angus, R. Clark, and A. Dzurak, Appl. Phys. Lett. **94**, 173502 (2009).

[23] P. C. Spruijtenburg, S. V. Amitonov, W. G. van der Wiel, and F. A. Zwanenburg, Nanotechnology **29**, 143001 (2018).

[24] See Supplemental Material at http://link.aps.org/supplemental/10.1103/PhysRevB.100.165305 for details regarding device fabrication, measurements, and analysis.

[25] S. Jung, T. Fujisawa, Y. Hirayama, and Y. Jeong, Appl. Phys. Lett. **85**, 768 (2004).

[26] C. W. J. Beenakker, Phys. Rev. B **44**, 1646 (1991).

[27] F. Beaudoin and W. A. Coish, Phys. Rev. B **91**, 165432 (2015).

[28] C. Buizert, F. H. L. Koppens, M. Pioro-Ladrière, H.-P. Tranitz, I. T. Vink, S. Tarucha, W. Wegscheider, and L. M. K. Vandersypen, Phys. Rev. Lett. **101**, 226603 (2008).

[29] Ç. Kurdak, C.-J. Chen, D. C. Tsui, S. Parihar, S. Lyon, and G. W. Weimann, Phys. Rev. B **56**, 9813 (1997).

[30] J. L. Black and B. L. Gyorffy, Phys. Rev. Lett. **41**, 1595 (1978).

[31] K. Agarwal, I. Martin, M. D. Lukin, and E. Demler, Phys. Rev. B **87**, 144201 (2013).

[32] R. W. Simmonds, K. M. Lang, D. A. Hite, S. Nam, D. P. Pappas, and J. M. Martinis, Phys. Rev. Lett. **93**, 077003 (2004).

[33] J. Lisenfeld, C. Müller, J. H. Cole, P. Bushev, A. Lukashenko, A. Shnirman, and A. V. Ustinov, Phys. Rev. Lett. **105**, 230504 (2010).

[34] G. J. Grabovskij, T. Peichl, J. Lisenfeld, G. Weiss, and A. V. Ustinov, Science **338**, 232 (2012).

[35] T. C. DuBois, M. C. Per, S. P. Russo, and J. H. Cole, Phys. Rev. Lett. **110**, 077002 (2013).

[36] M. Hauck, F. Seilmeier, S. E. Beavan, A. Badolato, P. M. Petroff, and A. Högele, Phys. Rev. B **90**, 235306 (2014).

[37] M. Pioro-Ladrière, J. H. Davies, A. R. Long, A. S. Sachrajda, L. Gaudreau, P. Zawadzki, J. Lapointe, J. Gupta, Z. Wasilewski, and S. Studenikin, Phys. Rev. B **72**, 115331 (2005).

[38] E. Burstein and A. L. McWhorter, in *Semiconductor Surface Physics*, edited by R. H. Kingston (Literary Licensing, LLC, 2012).

[39] U. Güngördü and J. P. Kestner, Phys. Rev. B **99**, 081301(R) (2019).

[40] O. E. Dial, M. D. Shulman, S. P. Harvey, H. Bluhm, V. Umansky, and A. Yacoby, Phys. Rev. Lett. **110**, 146804 (2013).

[41] D. Fleetwood, IEEE Trans. Nucl. Sci. **62**, 1462 (2015).

[42] G. Liu, S. Rumyantsev, M. A. Bloodgood, T. T. Salguero, M. Shur, and A. A. Balandin, Nano Lett. **17**, 377 (2016).

[43] D. Fleetwood, T. Postel, and N. Giordano, J. Appl. Phys. **56**, 3256 (1984).

[44] J. Burnett, L. Faoro, and T. Lindström, Supercond. Sci. Technol. **29**, 044008 (2016).

[45] A. L. Burin, S. Matityahu, and M. Schechter, Phys. Rev. B **92**, 174201 (2015).

[46] J. M. Martinis, K. B. Cooper, R. McDermott, M. Steffen, M. Ansmann, K. D. Osborn, K. Cicak, S. Oh, D. P. Pappas, R. W. Simmonds, and C. C. Yu, Phys. Rev. Lett. **95**, 210503 (2005).

[47] B. Sarabi, A. N. Ramanayaka, A. L. Burin, F. C. Wellstood, and K. D. Osborn, Phys. Rev. Lett. **116**, 167002 (2016).

[48] N. M. Zimmerman, C.-H. Yang, N. S. Lai, W. H. Lim, and A. S. Dzurak, Nanotechnology **25**, 405201 (2014).